Uranium speciation in two Freital mine tailing samples: EXAFS, μ-XRD, and μ-XRF results

Andreas C. Scheinost[1,2], Christoph Hennig[1,2], Andrea Somogyi[3], Gemma Martinez-Criado[4], Reinhard Knappik[5]

[1]Institute of Radiochemistry, FZR, Dresden, Germany,
[2]The Rossendorf Beamline at ESRF, Grenoble, France, E-mail: scheinost@esrf.fr
[3]Synchrotron Soleil, Gif-sur-Yvette, France
[4]ESRF, ID-22, Grenoble, France
[5]VKTA Rossendorf, Dresden, Germany

Abstract. We investigated the uranium speciation in a former WISMUT mine tailing, which was buried for 30 years under mine and construction debris. Chemical extractions, EXAFS, μ-XRD, and μ-XRF reveal two major U pools. The first with a relatively high potential mobility was identified as U(VI) sorbed to layer silicates by inner-sphere complexation; the second pool is represented by the relatively insoluble U(IV) minerals pitchblende and coffinite, and by the U(VI) solids uranyl hydroxide and vanuralite. Distribution between the two pools seems to be controlled by pH. Evidence for reductive precipitation of uraninite was found.

Introduction

During uranium ore extraction, uranium is converted from relatively insoluble U(IV) and U(VI) minerals to highly soluble U(VI) species. Contaminated mine waste piles, tailings and surrounding soils are usually covered by soil material to reduce the Rn emission and radionuclide spreading by wind and water erosion. Under these conditions, microbial and surface-catalytic reduction may transform uranium back to more immobile, tetravalent or hexavalent species. The mechanisms and kinetics of such processes are largely unknown, but are crucial to predict the long-term risks associated with mining sites, nuclear waste repositories and other contaminated sites.

In spite of their environmental relevance, only few studies succeeded to reliably identify uranium species in contaminated soils and sediments. Hunter and Bertsch (1998) found uranyl hydroxide phases and U(VI) associated with organic matter

and amorphous Fe oxides in soils at the Savannah River DOE site. Morris et al. (1996) found autunite- and schoepite-like phases in soils of at Fernald (Ohio). Roh et al. (2000) found schoepite, uranophane, coffinite, U-Ca-oxide and U-Ca-phosphates at Oak Ridge (Tennessee). Catalano et al. (2004) found boltwoodite in sediments at Hanford (Washington). Here we present the first study on U speciation at a former WISMUT (Germany) uranium mining and extraction site, which had been covered for 30 years.

Metal speciation in soils and sediments is a difficult task, since commonly several aqueous, sorbed and mineral species coexist (Manceau et al. 1996; Scheinost et al. 2002). This may be especially true for uranium mining sites, which reflect the rich mineralogy of the Saxonian Erzgebirge. Therefore, we had to combine synchrotron microfocus techniques (μ-XRF and μ-XRD) with bulk X-ray absorption spectroscopy (XAS) and chemical extraction techniques to decipher uranium speciation along a depth profile of a former mine tailings.

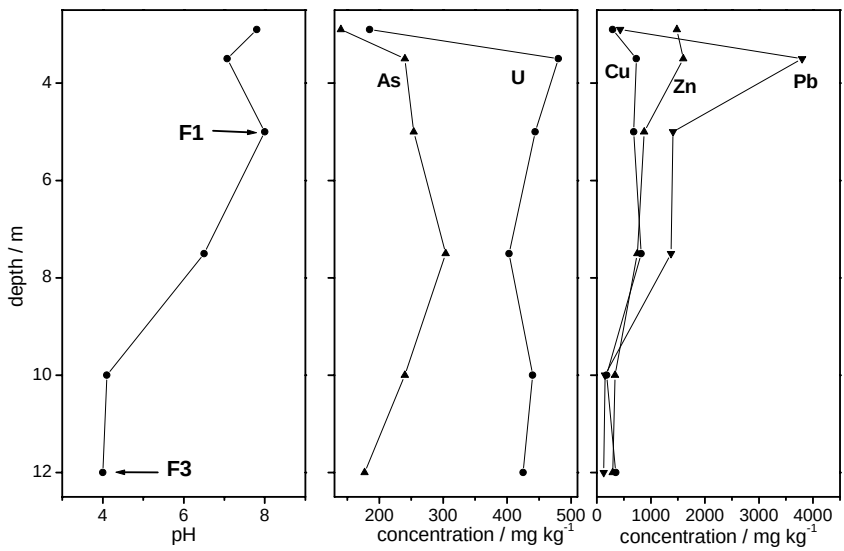

Fig. 1. Depth profiles of pH, U, As, Cu, Zn and Pb concentrations at Freital Tailings 1. The sampling depth of samples F1 and F2 is indicated by arrows.

Samples

Sediment cores were collected in 1992 at tailings 1 of the former Wismut operation site Freital near Dresden, Germany (Knappik et al. 1996). The mine tailings were used from 1949 to 1960 for ore-extraction wastes, and were covered from 1968 on by communal waste (mostly construction debris) and soil, followed by a second cover of mine debris. Samples F1 and F3 were collected at 5 and 12 m depth, respectively (Fig.1). The low pH of 4 at depths below 10 m reflects the former hydrochloric-acid ore-extraction procedure as well as pyrite oxidation and concomitant sulfuric acid release. At smaller depth, the construction debris and tin mine waste used for covering the tailings have created a neutralizing infiltration front with pH values as high as 8. The high pH is associated with high calcium contents, resulting from construction debris, and with high sulfur contents from pyrite oxidation. The cover by mine debris is most likely responsible for the peak concentrations of copper, zinc and lead at 4 m depth, which then decrease with increasing depth. Uranium concentrations vary between 400 and 500 mg/kg at selected sampling depths, while arsenic concentrations are roughly half of uranium concentrations.

Selective sequential extractions

Selective sequential extractions (SSE) were performed with a 7 step procedure (Zeien and Brümmer 1989): **1.** Water soluble salts and exchangeable ions: 1 M NH_4NO_3. **2.** Weakly complexed ions (often specific sorption): 1 M NH_4OAc at pH 6.0**. 3.** Metals bound by Mn hydroxides: 0.1 M NH_2OH-HCl + 1 M NH_4OAc at pH 6.0 and 5.5, resp. **4.** Strongly complexed metals (bound to organic matter): 0.025 M NH_4-EDTA at pH 4.6. **5.** Metals bound by easily reducible Fe(III) minerals: 0.2 M NH_4-oxalate at pH 3.25. **6.** Metals bound by other reducible Fe(III) minerals: 0.1 M ascorbic acid + 0.2 oxalate at pH 3.25. **7.** Recalcitrant minerals: microwave digestion. Total elemental concentrations were determined by ICP-MS, and complemented by graphite furnace AAS and energy-dispersive XRF analysis (Spectro XLab 2000).

The selective sequential extraction results suggest that in sample F1 (pH 8) the predominant part of U is highly mobile, while in F3 (pH) most U is strongly bound by recalcitrant mineral phases (Fig.2). Other mobile metals include Ni, Cu and Zn, while Th and Pb are bound by recalcitrant mineral phases. Therefore, U, Ni, Cu and Zn are susceptible to leaching from these tailings.

EXAFS spectroscopy

Bulk U L_{III}-edge X-ray absorption fine structure (EXAFS) spectra were collected at the Rossendorf Beamline (BM20, ESRF) at room temperature using a 13-element Ge fluorescence detector (Canberra) with digital signal processing (XIA). In spite of the enhanced energy resolution of this detector, the U-L_{III} line was partly hidden behind the strong K-lines of Rb and Sr, preventing collection of high quality spectra (Fig.3). Hence unweighted U L_{III}-edge EXAFS spectra of F1 and F3 were analyzed by linear combination fits using an EXAFS data base of 60 references encompassing aqueous, sorbed and mineral species. The best fit results

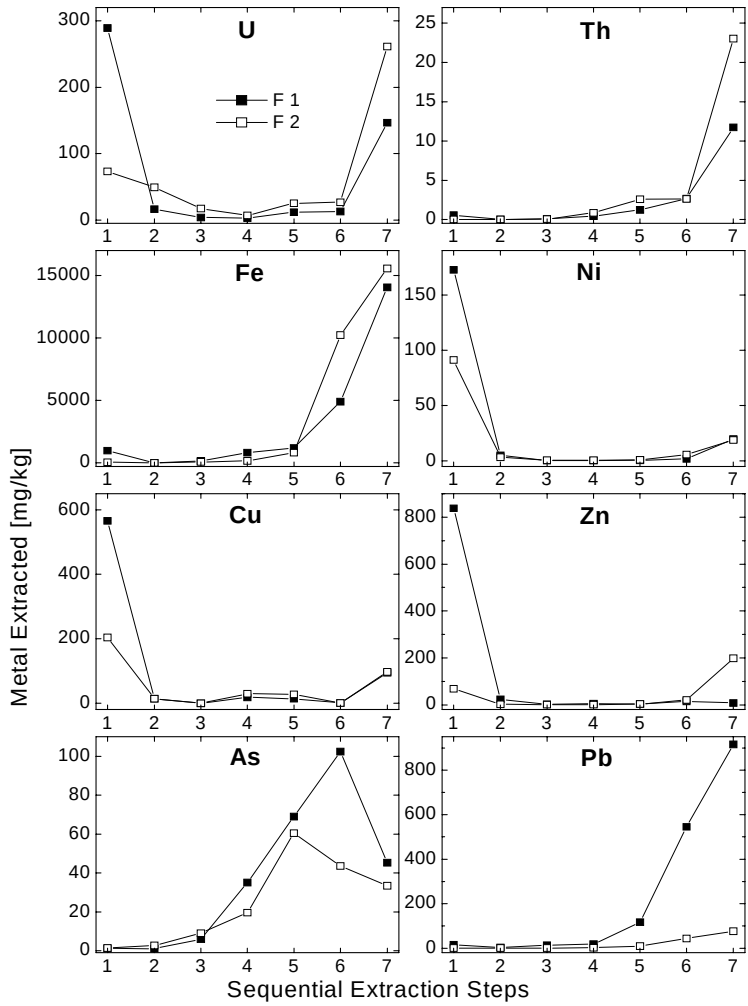

Fig. 2. Selective sequential extraction results of samples F1 and F3.

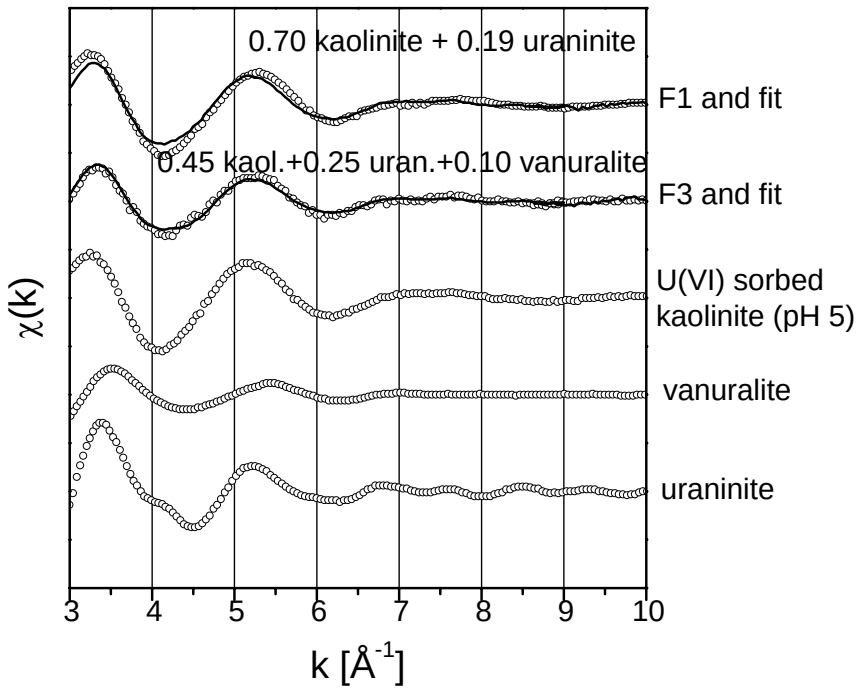

Fig. 3. Uranium L_{III}-edge EXAFS spectra of F1 and F3, their best linear combination fits, and the EXAFS spectra of selected uranium references.

suggest that F1 contains 70 % of total U sorbed as U(VI) innersphere sorption complexes on kaolinite or clay minerals with similar edge sites, and 20 % bound by uraninite. The fit results of F3 suggest a smaller amount of sorbed U(VI) and more uraninite as in F1, and an additional mineral phase, vanuralite (Fig.3).

Synchrotron μ-XRF and μ-XRD

Micro-XRF and μ-XRD was performed on beamline ID-22 (ESRF), using KB-mirrors to focus the beam size to 2 x 6.7 μm^2. Micro-XRF spectra were collected with a SiLi detector. Clay-sized samples were sprinkled on Kapton tape. Elemental maps were produced from 2-dimensional micro-XRF arrays by deconvolution of the fluorescence lines with AXIL (University of Antwerp). Micro-XRD Laue patterns were collected with a CCD camera positioned 60 mm behind the sample and normal to the incident beam. An incident energy of 18 keV, corresponding to a wavelength of 0.6887 Å was used. The camera 2-d images were converted to powder patterns with Fit2D (A. Hammersley, ESRF) and then analyzed by the search software EVA (Siemens).

Fig.4 shows elemental distribution and elemental associations as tricolor maps, i.e. the concentration of selected elements is coded by one of the colors red, green

and blue. In sample F1, closely associated U and Cu (U/Cu, r=0.84) occur predominately in K-rich aggregates with diameters of tens to hundreds of μm, creating purplish hues (Fig.4 left). Uranium concentrations in these regions are in the mg/kg range, suggesting either minerals where U is not a substantial component or U sorption complexes. In addition, U occurs as small crystals without any other heavier (≥Si) elements (red dots), presumably uranium oxides.

Elongated areas with close association of Ca and S suggest gypsum (green), blue regions indicate feldspar minerals. In sample F3, U does not show strong correlations with other elements across the whole map (Fig.4 right), indicating a varied U mineralogy or sorption to various minerals. In two larger aggregates, U (and Cu, Z, Ni) are associated with K as in F1. However, other U-rich areas are associated with V (purplish regions), Cu (yellow) or Ca (not shown). Again, in some small spots U is not associated with other elements ≥ Si. Uranium concentrations are often in the g/kg range suggesting the presence of U minerals.

Based on this elemental mapping, single spots containing U were selected for μ-XRD. The μ-XRF spectra of these spots are shown in Fig.5, the corresponding mineral composition as derived from μ-XRD patterns is given in Table 1. The μ-XRF spectra demonstrate the relatively homogenous elemental composition of spots in F1, while spots in F3 have differing elemental compositions. The μ-XRD Laue patterns of F1 show predominately ring patterns suggesting an assembly of particles within the probed spot size, while those of F3 show both powder and single-crystal patterns (data not given). Hence μ-XRF and μ-XRD both confirm that U in F1 is associated with mineral aggregates with diameters of tens of micrometers, while U in F3 is associated with both single crystals and with mineral aggregates.

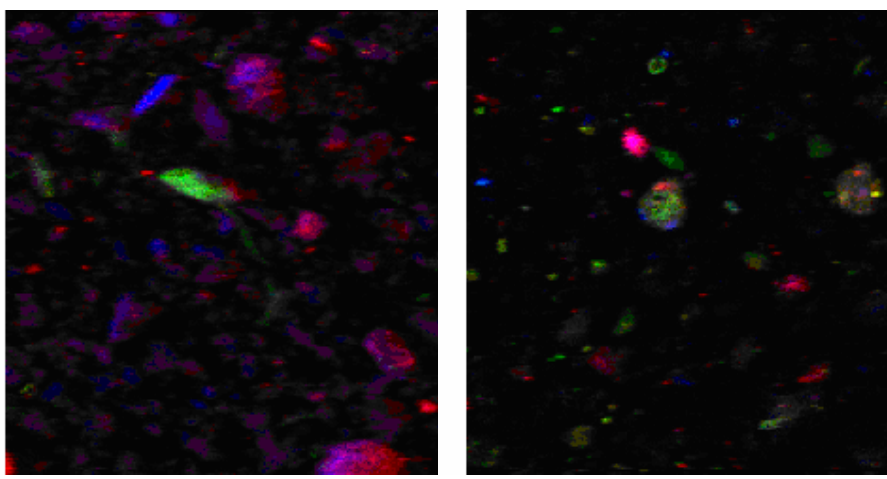

Fig. 4. Synchrotron μ-XRF maps (400x400 μm^2) of samples F1 (left) and F3 (right). The color encoding for F1 is U (red), K (blue), S (green). The color encoding for F3 is U (red), Cu (green), V (blue).

The bulk mineral composition of both samples consists of quartz and phyllosilicates; F1 shows in addition gypsum, and F2 in addition feldspar (Table 1). In F1, μ-XRD revealed in addition to the bulk minerals jarosite, but no U minerals. Together with the large amount of exchangeable U (Fig.2) and its diffuse distribution within K-rich aggregates (Fig.4), this suggests that most U is sorbed onto the edge sites of phyllosilicates in F1. This is in line with bulk-EXAFS suggesting formation of inner-sphere sorption complexes on kaolinite. At pH 8, high [HCO_3^-] could prevent U(VI) sorption due to formation of neutral aqueous carbonato complexes, but since [HCO_3^-] is low (<0.5 mg/L) (Knappik et al. 1996) sorption takes place. Both μ-XRF and EXAFS suggest also a smaller amount of U oxide/uraninite, which was not detected by μ-XRD. The large secondary gypsum precipitates found in this sample contain only a very minor amount of U, hence do not constitute a relevant sink for U.

In F3, the U(IV) minerals coffinite and uraninite, and the U(VI) minerals uranyl hydroxide and vanuralite were identified. In addition, a smaller part of U is

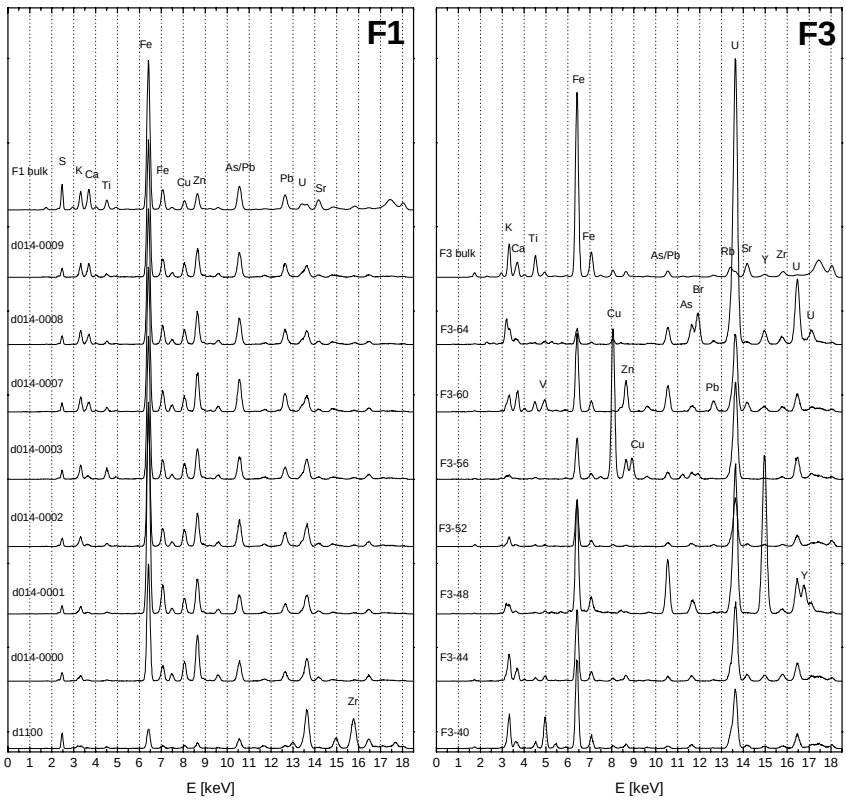

Fig. 5. Bulk XRF and synchrotron μ-XRF spectra of selected spots of samples F1 and F3. The corresponding mineral composition as derived from μ-XRD is given in Table 1.

again associated with phyllosilicate minerals suggesting sorption (Table 1).

While we found four U minerals with μ-XRD, we could confirm only two minerals, uraninite and vanuralite, by linear combination fit of EXAFS spectra (Fig.3), although reference spectra for the other phases were available and were tested as targets. While this could be due to the limited EXAFS data quality achievable with such difficult samples, it may also suggest that the total amount of U in coffinite and uranyl hydroxide is below the detection limit of the bulk EXAFS method.

At the low pH of 4, specific sorption of uranyl ions to the variable-charge edge sites of phyllosilicates is reduced due to competition with protons. Hence we considered non-specific sorption to permanent-charge phyllosilicates like montmorillonite as an alternative. Such minerals were not identified by XRD and μ-XRD (Table 1). Furthermore, linear combination fits of the EXAFS spectra revealed the presence of U-sorbed kaolinite (Fig.2), while U-sorbed montmorillonite gave a significantly poorer fit. Hence in spite of the relatively low pH, formation of inner-sphere sorption complexes seems to be the prevalent sorption process because of the lack of permanent-charge phyllosilicates.

While the limited number of spots investigated by μ-XRF may not provide a statistically reliable U speciation in F3, the prevalence of U in recalcitrant mineral phases is confirmed by the two bulk methods, SSE and EXAFS. The small amount of U minerals is far below the detection limit of bulk XRD.

In terms of remediation strategies and the geochemical kinetics of U cycles, it would be important to know, if the identified U minerals are primary phases left behind by an incomplete extraction of the ore, or if they are secondary minerals formed from soluble U(VI) by precipitation and reduction-precipitation. The main U ore extracted at the Freital site was pitchblende associated with local coal deposits, but also pitchblende from other Saxonian and Thuringian mining locations, hence the identified uraninite could have been inherited from the ore. However, EXAFS spectra of seven natural pitchblende samples from Erzgebirge and worldwide sources revealed significant fractions of U(VI) due to oxidation (not shown), and did not fit the EXAFS spectra of F1 and F3. In contrast, a synthetic uraninite sample with a composition close to UO_2 gave a reasonable fit of the sample spectra (Fig.3). This suggests that the observed uraninite could be in fact a recent secondary precipitate, formed most likely after microbial reduction of soluble U(VI).

As minor fractions, coffinite and vanuralite were also minerals of the U ore. Both may have resisted the acidic ore extraction procedure, hence are most likely inherited. At one spot in F3, the synthetic phase uranyl hydroxide was identified (card 70-1520), which is most likely a secondary precipitate, but of only minor importance for the U mineralogy due to its small abundance.

Table 1. Mineral phases identified in bulk samples and in selected spots by μ-XRD.

Sample	main elements	identified phases
F1-bulk		Qz, muscovite, (illite), kaolinite, gypsum
F1-d1100	S, Fe, As, Pb, Bi, U, Y/Rb, Zr	(Qz), muscovite, (jarosite)
F1-d014-00	S, K, Fe, Ni, Cu, Zn, Pb, U	(Qz), kaolinite, muscovite, jarosite
F1-d014-01	d014-00	(Qz), kaolinite, muscovite, jarosite
F1-d014-02	d014-00 +Ti	kaolinite, muscovite, (illite), jarosite
F1-d014-03	d014-00 +Ti	(Qz), kaolinite, muscovite, jarosite
F1-d014-07	d014-00 +Ca +Ti	(Qz), kaolinite, muscovite, (illite) , gypsum, jarosite
F1-d014-08	d014-00 +Ca +Ti	(Qz), kaolinite, muscovite, (illite) , gypsum, jarosite
F1-d014-09	d014-00 +Ca +Ti	(Qz), kaolinite, muscovite, gypsum, jarosite
F3-bulk		Qz, microcline, kaolinite, muscovite, (illite)
F3-d040	K, V, Fe, U	Qz, muscovite, (illite), hematite, **vanuralite** ($Al(UO_2)_2V_2O_8(OH)$ x $11H_2O$)
F3-d044	K, Ca, Fe, U	Qz, muscovite , (**uraninite), (uranyl hydroxide)**
F3-d048	K, Fe, As, U, Y	(Qz), hematite, **uraninite**, xenotime
F3-d052	K, Fe, U	muscovite, (illite), **uraninite, uranyl hydroxide**
F3-d056	Fe, Cu, Cr, U	(Qz), muscovite, (illite)
F3-d060	K, Ca, Ti, V, Fe, Zn, As, Pb, U	(Qz), muscovite, (illite)
F3-d064	K, Ca, Fe, Br, U	Qz, **coffinite**

Conclusions

At smaller depth (F1, 5 m), hydrochloric acid from the ore extraction and sulfuric acid from pyrite oxidation was completely neutralized by the construction debris used as cover material, resulting in precipitation of jarosite and gypsum. The predominant uranium species at this depth is U(VI) sorbed to variable-charge sites of clay minerals. At greater depth (F3, 12 m), the low pH from ore extraction was conserved. The predominant part of U is hosted by U(IV) and U(VI) minerals. While coffinite and vanuralite are most likely inherited from the U ore, evidence of uraninite with a formal U oxidation state close to 4 suggests a reduction and precipitation process in the tailings sediments. The U minerals were recalcitrant during chemical extractions, indicating low uranium solubility even at oxic redox conditions. Hence the results demonstrate a potentially high mobility of U at lower depth and high pH, while U at greater depth and low pH is hosted by low-soluble minerals, which in part may have formed by a natural (microbial) attenuation mechanism within the 50 to 30 years since the deposition of the mine tailings. The high spatial variability of geochemical parameters in such tailings, the related variability of uranium speciation, and finally the kinetic aspects of mineral disso-

lution/precipitation have to be considered by coupled kinetic geochemical and transport models, posing a substantial challenge for reliable risk assessments.

Acknowledgements

We thank M. Leckelt, U. Schäfer, A. Scholz, Dr. K. Krogner and Dr. F. Prokert (all FZR) for their help with sample and data analyses. Prof. Vochten (Univ. Antwerp) and A. Massanek (TU Freiberg) shared their large collections of reference U minerals. The European Synchrotron Radiation Facility provided access to the microfocus beamline ID-22.

References

Catalano J G, Heald S M, Zachara J M, Brown G E (2004) Spectroscopic and diffraction study of uranium speciation in contaminated vadose zone sediments from the Hanford site, Washington state. Environmental Science & Technology 38(10): 2822-2828.

Hunter D B, Bertsch P M (1998) In situ examination of uranium contaminated soil particles by micro-X-ray absorption and micro-fluorescence spectrocopies. Journal of Radioanalytical and Nuclear Research 234(1-2): 237-242.

Knappik R, Mocker D, Friedrich H-J. (1996) Migrationsverhalten von Radionukliden in Tailings unter besonderer Berücksichtigung des Oxidationspotentials in alten Tailingsablagerungen. VKTA Rossendorf.

Manceau A, Boisset M C, Sarret G, Hazemann J L, Mench M, Cambier P, Prost R (1996) Direct determination of lead speciation in contaminated soils by EXAFS spectroscopy. Environmental Science & Technology 30: 1540-1552.

Morris D E, Allen P G, Berg J M, ChisholmBrause C J, Conradson S D, Donohoe R J, Hess N J, Musgrave J A, Tait C D (1996) Speciation of uranium in Fernald soils by molecular spectroscopic methods: Characterization of untreated soils. Environmental Science & Technology 30(7): 2322-2331.

Roh Y, Lee S R, Choi S K, Elless M P, Lee S Y (2000) Physicochemical and mineralogical characterization of uranium-contaminated soils. Soil & Sediment Contamination 9(5): 463-486.

Scheinost A C, Kretzschmar R, Pfister S, Roberts D R (2002) Combining selective sequential extractions, X-ray absorption spectroscopy and principal component analysis for quantitative zinc speciation in soil. Environmental Science & Technology 36(23): 5021-5028.

Zeien H, Brümmer G W (1989) Chemische Extraktion zur Bestimmung von Schwermetallbindungsformen in Böden. Mitteilungen der Deutschen Bodenkundlichen Gesellschaft 59(1): 505-510.